STRONG FIELD INTERACTIONS WITH ATOMS AND MOLECULES

SUSANA ARIAS LASO

A DISSERTATION SUBMITTED TO
THE FACULTY OF GRADUATE STUDIES
IN PARTIAL FULFILLMENT OF THE REQUIREMENTS
FOR THE DEGREE OF
DOCTOR OF PHILOSOPHY

GRADUATE PROGRAM IN PHYSICS AND ASTRONOMY
YORK UNIVERSITY
TORONTO, ONTARIO

May 19, 2020

Abstract

this is the abstract

Contents

List of Tables

List of Figures

1 Introduction

ref [1]

2 Electronic Structure of H_2O

2.1 Variational Hartree-Fock Method

2.2 Self-Consistent Field Slater Orbitals

3 H_2O in an external electric dc field

The dc Stark problem for the H_2O valence orbitals is addressed in this chapter through the implementation of a complex scaling approach that allows to study the effect of an external dc field on each molecular orbital independently. The construction of an effective potential that reflects the indivual properties of the orbitals is crucial in this analysis.

3.1 Molecular structure of H_2O

3.2 Partial differential equation approach to the problem

3.2.1 Exterior complex scaling

3.3 Stark resonance parameters

3.3.1 $1b_1$ and $1b_2$ molecular orbitals

3.3.2 $3a_1$ molecular orbital

4 Above threshold ionization in laser-atom and laser-molecule interactions

The phenomenon of above threshold ionization (ATI) [2] has been tackled through diverse approaches, with analytical approximations dating back to Keldysh theory of strong-field approximation [3]. Alternatively, attempts to find a numerical solution to the time-dependent Schrödinger equation (TDSE) [4–6] have been instrumental for the understanding of ATI, and a variety of efforts that deal with the complexity of solving this challenging numerical problem have been successful in the past [7]. In the same way, complementary approaches to the solution of the TDSE, such as the so-called Volkov-based methods [8–10], have revealed their strengths within strong-laser field problems in which a numerical solution would involve a computationally taxing problem. The strong-field approximation [3], which considers the binding potential as a perturbation, is the foundation to the formalism discussed in this chapter.

Sec. 4.1 presents an overview of the pioneering work by Keldysh which introduces the strong-field approximation to describe the laser ionization of atoms. Next, a generalized approach that introduces rescattering of the electron back to the vicinity of the binding potential is included in Sec. 4.2. The ionization regime of a model He atom under a strong-laser field is explored in Sec. 4.3.1 for both scenarios: considering only direct electrons where the ionization spectrum is reproduced by the Keldysh amplitude, and using a compact expression for the transition amplitude that encloses the limiting case of direct trajectories while allowing electrons to rescatter to the parent ion as well. Additionally, this study is extended to explore the laser ionization of the $1b_1$ and $1b_2$ molecular orbitals of H_2O in Sec. 4.3.2. The analysis presented in this chapter closely follows that of [11].

4.1 Keldysh formalism

In the Keldysh theory of strong-field approximation [3] the common nature of both competing effects multiphoton ionization and tunneling ionization is illustrated. These limiting cases of strong-field ionization are accounted for provided the laser lies in the low-frequency region, $\omega \ll \omega_t$, where ω_t indicates the tunneling frequency, in which the tunnel effect prevails, or the high-frequency region, $\omega \gg \omega_t$, in which multiphoton absorption takes place. Commonly, the Keldysh parameter defined as the ratio of the frequency of the laser field to the tunneling rate, $\gamma = \sqrt{I_p/(2U_p)}$, where I_p is the atomic ionization potential and $U_p = I/4\omega^2$ is the ponderomotive energy of a free electron in the laser field of frequency ω and intensity I, indicates the dominant mechanism by taking values larger or smaller than 1. In contrast with the tunneling regime, in which the tunnel effect is determined solely by the field intensity, at higher frequencies the tunneling probability is no longer constant and the transition of the electron into a free state is accompanied by a competing mechanism in which several photons are absorved simultaneously.

Even though the Keldysh formalism for strong-field ionization provided very good agreement with experimental data of electron ATI spectra for helium ionization at relatively low energies [12], rescattering effects were not included in the theory and it fails to reproduce the rescattering induced plateau that is visible in measurements along a broader energy spectrum [13]. In this chapter we are concerned with the numerical evaluation of an improved Keldysh approximation [11] that accounts for rescattering and reveals the complex structure of the ionization spectrum.

The probability amplitude for an electron to transfer from the ground state of an atom with binding potential $V(\mathbf{r})$ into a scattering state $|\psi_{\mathbf{p}}(t)\rangle$ due to an external laser field is given by [11]

$$M_{\mathbf{p}} = \lim_{t\to\infty, t'\to-\infty} \langle \psi_{\mathbf{p}}(t)|U(t,t')|\psi_0(t')\rangle, \tag{4.1}$$

where it is assumed that in the limit of early times, $t' \to -\infty$, the exact wave function reduces to the unperturbed wave function $\psi_0(t)$ of the initial ground state. Here the evolution operator formalism is implemented by means of the time-evolution operator, $U(t,t')$, in order to obtain a formal expression for the transition amplitude in which the total wave function is represented in terms of the unperturbed wave function. In the problem that concerns us, the time-evolution

operator propagates the wave function $|\psi(t)\rangle$ from t' to t under the full Hamiltonian

$$H(t) = -\frac{1}{2}\nabla^2 + H_I(t) + V(\mathbf{r}) \tag{4.2}$$

that includes the binding potential, $V(\mathbf{r})$, of the parent ion and the interaction with the laser field, $H_I(t) = -\mathbf{r}\cdot\mathbf{E}(t)$, under the dipole approximation in the length gauge [11].

The time-evolution operator satisfies an integral equation, namely the Dyson equation [11, 14], which conveniently allows to construct an expansion in which the interaction with the external field is treated as a perturbation. This representation, together with the orthogonality of the initial ground state $|\psi_0\rangle$ and scattering state $|\psi_\mathbf{p}\rangle$, illustrates the possibility of major excursions of the scattering electron away from its parent ion once it was propagated from the initial state by $U(t,t')$.

Two approximations are crucial to derive the Keldysh result for the transition amplitude [11]. The first approximation consists of replacing the complete time-evolution operator in (4.1) by the Volkov time-evolution operator $U^V(t,t')$, which propagates the wave function of a free electron coupled through the interaction $H_I(t)$ to the external laser field. In other words, the interaction with the binding potential is considered a perturbation everywhere except in the initial and final states. In the second approximation the scattering state, $\psi_\mathbf{p}$, is replaced by the Volkov wave function, $\psi_\mathbf{p}^{(V)}$, which represents the state of a free electron in a laser field with time-averaged momentum $\mathbf{p}$. Further details about the derivation are to be found in [11]. These transformations, along with additional algebraic operations, lead to obtain an equivalent form of the standard Keldysh amplitude [11, 15]

$$M_\mathbf{p}^{(0)} = -i\int_{-\infty}^{\infty} dt\ \langle\psi_\mathbf{p}^{(V)}(t)|V|\psi_0(t)\rangle. \tag{4.3}$$

Generally, replacing the time-evolution propagator $U(t,t')$ by the Volkov propagator $U^{(V)}(t,t')$ gains in precision the shorter the range of the binding potential and the higher the intensity of the laser field. In what follows we will consider the limiting case of zero-range interactions of the form

$$V(\mathbf{r}) = \frac{2\pi}{m\kappa}\delta(\mathbf{r})\frac{\partial}{\partial r}r, \tag{4.4}$$

which support a scattering state that approaches a plane wave except for an $s-$wave term [7, 16]. Zero-range potentials have been widely used in molecular and collision problems [17, 18], as well

as tunneling [19] and multiphoton problems [20]. Inserting the zero-range potential (4.4) into the Keldysh amplitude (4.3) yields the expansion

$$M_{\mathbf{p}}^{(0)} \sim \frac{m}{2\pi}\sqrt{2m|E_0|}\sum_n \delta\left(\frac{p^2}{2m} + U_p + |E_0| - n\omega\right) \times \sum_{l=-\infty}^{\infty} J_{2l+n}\left(\frac{2p_x}{\omega}\sqrt{\frac{U_p}{m}}\right) J_l\left(\frac{U_p}{2\omega}\right), \tag{4.5}$$

that generates the ionization spectrum of direct electrons only [11]. Here U_p represents the ponderomotive potential of an electron moving in the laser field with momentum $\mathbf{p}$ parallel to the laser field, $p_x = |\mathbf{p}|$, $|E_0|$ stands for the binding energy, and the J_n represent Bessel functions.

4.2 Generalized ionization amplitude including rescattering

In order to include electron rescattering in our study, it is necessary to allow the electron to interact with the parent ion once it has been freed from the binding potential. This represents a step further in relation to Keldysh theory of direct ionization [3] and it can be implemented by resorting to the Dyson expansion of the time-evolution operator in which the binding potential is considered a perturbation and the Volkov time-evolution operator plays an essential role. Inserting the expansion for the time-evolution operator into the ionization amplitude (4.1) one obtains the generalized expression [11]

$$\begin{aligned} M_{\mathbf{p}} = \; & -i\lim_{t\to\infty}\int_{-\infty}^{t} dt' \langle\psi_{\mathbf{p}}(t)|U^{(V)}(t,t')\{H_I(t')|\psi_0(t')\rangle \\ & -i\int_{-\infty}^{t'} dt'' V U(t',t'') H_I(t'')|\psi_0(t'')\rangle\}, \end{aligned} \tag{4.6}$$

which is still an exact representation of the transition amplitude. The first term is the direct amplitude that yields the Keldysh matrix element discussed in Sec. 4.1. The second term allows for additional interactions with the atomic potential, and therefore describes rescattering of the electron. Further algebraic transformations on the second term result in the compact expression for the ionization amplitude [11]

$$M_{\mathbf{p}} = -\int_{-\infty}^{\infty} dt \int_{-\infty}^{t} dt' \langle\psi_{\mathbf{p}}^{(V)}(t)|V U^{(V)}(t,t') V|\psi_0(t')\rangle, \tag{4.7}$$

where the scattering state was replaced by a plane wave in order to carry out the limit of $t \to \infty$. This expression now describes both the direct electrons that depart from the atom without further interaction with the binding potential as well as the electrons that are promoted to the continuum at some time t', and propagate in the laser field until some later time t when they return to within the range of the binding potential, whereupon they rescatter into their final Volkov state.

Evaluation of the matrix element (4.7) can be very cumbersome for a finite-range binding potential. However, it simplifies noticeably in the limit of a zero-range potential of the form (4.4) where the spatial integrations become trivial. Expanding the Volkov wave function and time-evolution operator in terms of Bessel functions, one of the remaining quadratures over time can be carried out and yields the energy conserving $\delta-$function. Therefore, one quadrature is left to be carried out numerically,

$$\begin{aligned} M_{\mathbf{p}} \sim & \sum_n \delta\left(\frac{p^2}{2m} + U_p + |E_0| - n\omega\right) \sum_{l=-\infty}^{\infty} J_{2l+n}\left(\frac{2p_x}{\omega}\sqrt{\frac{U_p}{m}}\right) \\ & \times \int_0^{\infty} d\tau \left(\frac{im}{2\pi\tau}\right)^{3/2} \left(e^{-i[|E_0|\tau + l\delta(\tau)]}\right. \\ & \times \exp\left\{-iU_p\tau\left[1 - \left(\frac{\sin\frac{1}{2}\omega\tau}{\frac{1}{2}\omega\tau}\right)^2\right]\right\} \\ & \left. J_l\left(y(\tau)\frac{U_p}{\omega}\right) - J_l\left(\frac{U_p}{2\omega}\right)\right), \end{aligned} \tag{4.8}$$

where the real quantities $y(\tau)$ and $\delta(\tau)$ are defined via

$$y(\tau)e^{-i\delta(\tau)} = \frac{1}{2} - i\left(\sin\omega\tau - \frac{4\sin^2\omega\tau/2}{\omega\tau}\right)e^{-i\omega\tau}. \tag{4.9}$$

explain this, since you failed yourself understanding how this determines two real quantities

4.3 Results

4.3.1 Ionization regime. A systematic study

This section is concerned with the study of the ionization spectrum generated by a strong laser field acting upon an atom with a binding potential that is approximated as a zero-range potential. The external laser field is assumed to be turned off in the distant past and future, $t \to \pm\infty$. With this in mind, we carry out the numerical evaluation of the transition amplitudes (4.5) and (4.8)

monochromatic (called a continuous-wave laser field)

in which we concentrate on the case of a linearly polarized field of the form

$$\mathbf{A} = A_0 \hat{\mathbf{x}} \cos(\omega t). \tag{4.10}$$

Both contributions the one from direct electrons described by the Keldysh amplitude as well as that from rescattering electrons which interact one more time with the binding potential are considered when studying the convergence of the ATI matrix element that generates the ionization spectrum. Our calculation considers a laser field with $\hbar\omega = 1.58$ eV at 10^{15} W/cm^2 acting upon a He atom with $E_0 = -0.9$ a.u. as the binding energy.

explain this → intensity in atomic units so one realizes the relative strengths of laser & binding vs energy

an intensity of ...

The numerical evaluation of the remaining quadrature in Eq. (4.8) in terms of the travel time is not straightforward as the convergence of the solution indicates to be sensitive to the working precision requested. Given that the integrand is independent of the electron energy, associated with p_x in Eq. (4.8), a fixed value of the Bessel function order l would correspond to a single value of the integral. This allows us to explore the convergence of the individual integrals that form the sum over Bessel orders before assembling the results to be summed over the discrete energies given by n. In what follows, we will refer to the time integral as $F(l)$ by rewriting Eq. (4.8) as

$$M_{\mathbf{p}} \sim \lim_{|l|_{\max}\to\infty} \sum_n \delta\left(\frac{p^2}{2m} + U_p + |E_0| - n\omega\right) \sum_{l=-|l|_{\max}}^{|l|_{\max}} J_{2l+n}\left(\frac{2p_x}{\omega}\sqrt{\frac{U_p}{m}}\right) F(l). \tag{4.11}$$

In the process of studying the convergence of $F(l)$, we partitioned the integration interval into subintervals of $2\pi/\omega$ and explored the progression of the results as a function of how many intervals are included in the calculation as well as the working precision requested. A final interval following the $k-$th interval, $[2\pi/\omega(k-1), 2\pi/\omega k)$, that extends to $+\infty$ is included in the calculation. Additionally, in order to bypass the singularity at $\tau = 0$ due to the $1/\tau$ factor in $F(l)$, a coordinate transform of the form $x \to \sqrt{\tau}$ is implemented so that the integrand converges to a finite value as τ approaches zero. This special coordinate transform is suitable only for small values of τ given that losing the $1/\tau$ factor would slow down the convergence of the integrand to zero at larger times.

to study the convergence of the sum you are demonstrating

discrete

Figure 4.1 illustrates the evolution of punctual values of $F(l)$ for a set of l values, $|l| = [10, 40, 80]$, as the working precision is increased. For $l = 10$, a working precision of about 15 decimal points seems to not affect the evaluation of the integral. As l increases, the values of the integral deviate from the initial evaluation until they converge. This happens relatively quickly

$F(l) \to \infty$ ↑ Level

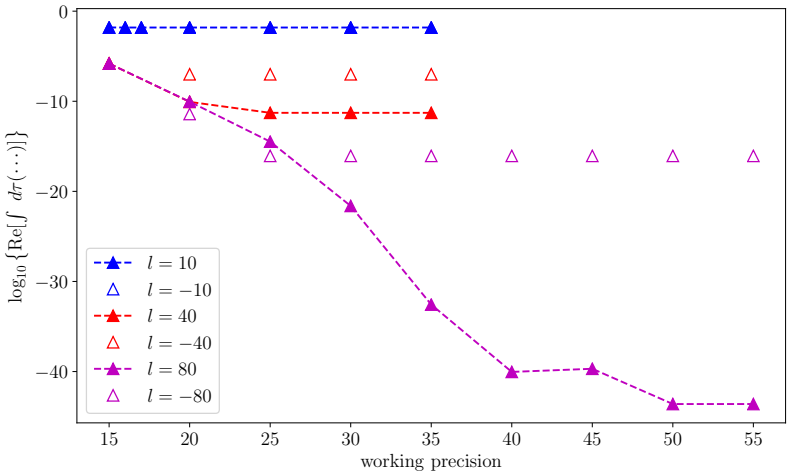

Figure 4.1: Numerical evaluation of the time integral $F(l)$ contained in the transition amplitude (4.11) for $|l| = 10, 40, 80$, indicated in blue, red and magenta respectively, as a function of the working precision requested.

for negative values of l for which the graphic indicates that approximately 25 digits of precision would be enough to obtain the converged result. In contrast, for $l > 0$ the digits of precision needed increased to 50 for $l = 80$.

Given that the transition amplitude that describes the rescattering of an electron to its binding potential (4.8) is a generalization of the Keldysh amplitude (4.5) one should expect that the generalized ATI spectrum contains that of direct electrons at low electron energies. A comparison between Eqs. (4.11) and (4.5) illustrates that, for a given value of l, the function $F(l)$ should be proportional to the Bessel factor $J_l\left(\frac{U_p}{2\omega}\right)$. This calculation was carried out for different values of l in order to corroborate the validity of the aforementioned generalization.

Figure 4.2 exhibits a comparison of the numerical evaluation of $F(l)$ in (4.11) with the simple Bessel function in (4.5) for several sets of increasing values of $l_{\max}$. The coefficients that replace the integral in the Keldysh amplitude were scaled, divided by a factor of 5, so it is possible to see the agreement. For negative values of l, at about $l = -30$, the curves begin to differ as the integrals oscillate around 10^{-6} (arb. units) for a range of negative l values that extends from $l \approx -30$ to $l \approx -60$, indicating the presence of rescattering as opposed to the case for

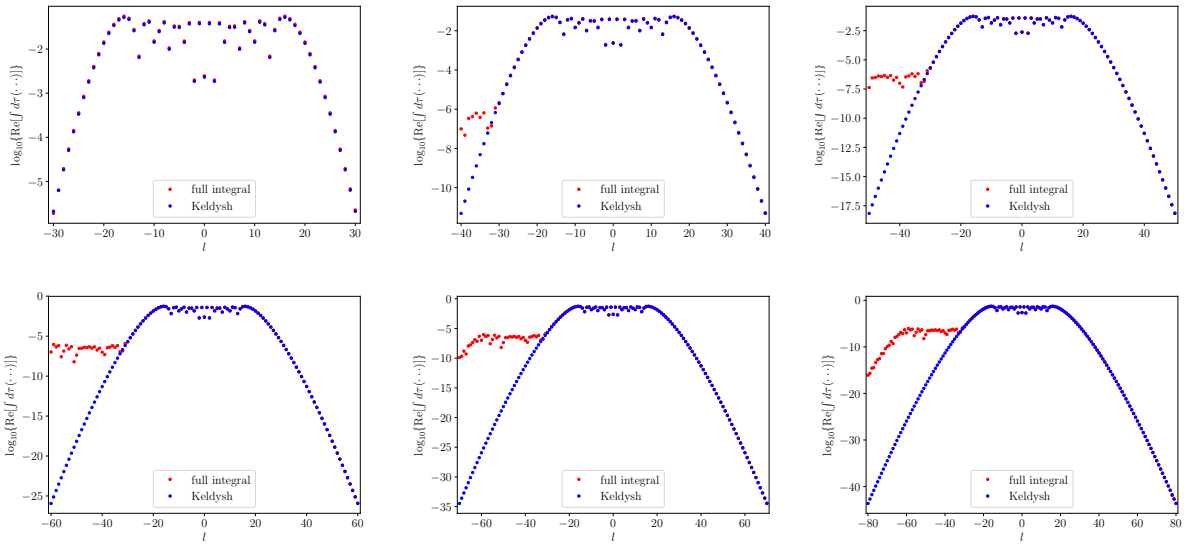

Figure 4.2: Numerical evaluation of the time integral $F(l)$ contained in the transition amplitude (4.11) (red dots) in contrast with its analogous Bessel term in the Keldysh amplitude for direct transmission (blue dots) for zero-range He atom model as a function of the Bessel function order l for increasing values of $l_{\max}$, $l = [-l_{\max}, \ldots, l_{\max}]$.

the direct transmission, shown as blue dots, from the Keldysh amplitude. As one might notice, for sufficiently small negative values of l ($l < -60$) the values of the integral start dropping below, indicating that convergence of the ionization spectrum for rescattering electrons is to be expected. As the Bessel order, l, was increased in the evaluation of the quadrature, the working precision and precision goal were tuned appropriately so the curves would remain comparable. This is consistent with Figure 4.1, as the order of Bessel functions increases, a higher working precision is required in order to find a numerical solution to the quadrature.

The ionization spectrum of ~~He~~ for the He model for emission parallel to the electric field of the laser that contains the contribution of direct electrons, given by the Keldysh amplitude (4.5), is shown in Figure 4.3. For a given electron energy, the sum over the Bessel order was extended up to increasing values of $l_{\max}$, ranging from 20 to 50, in order to display the convergence of the spectrum in the limit $l \to \infty$. For $l_{\max}$ values as low as 20 and 30 the final structure of the spectrum for very small energies, $< 1\mathrm{U_p}$, begins to be visible. However, more terms need to be considered in the sum over Bessel functions in order to obtain the converged spectrum. The yield

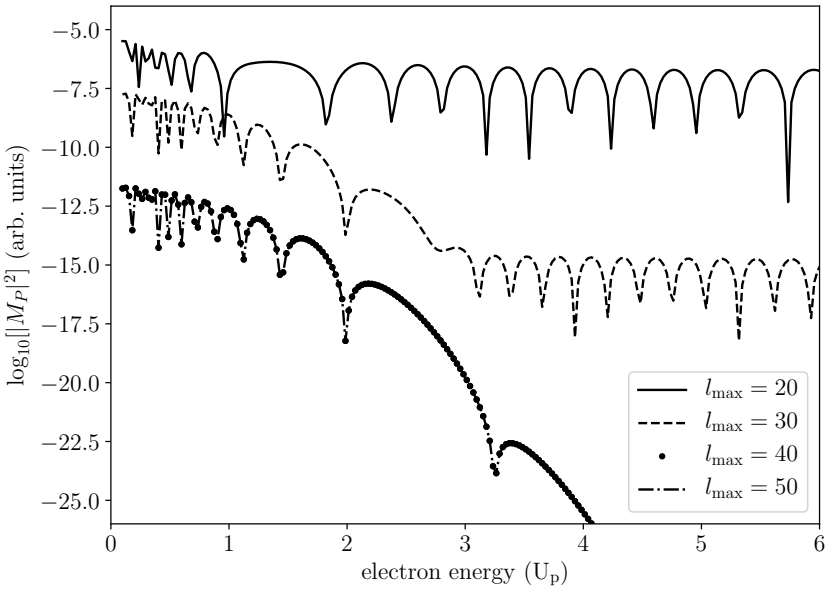

zero range model for

What are the laser parameters?

Figure 4.3: ATI spectrum of helium by a linearly polarized field describing direct electrons. Each curve corresponds to a finite value of $l_{\max}$ in the standard Keldysh amplitude.

consisting only of direct electrons converges relatively fast to its final shape (dash-dotted line) in which a sequence of narrow suppressions of the probability amplitude separated by rounded tops drops as the electron energy increases and eventually vanishes at about $2.5U_p$.

The results of the calculations based on (4.8) are shown in Figure 4.4. Each coloured curve represents the ionization amplitude for an atom of He under a strong laser field for increasing values of the Bessel function order, l. As one might notice, the ionization spectrum converges for $l = 80$ (bottom right plot) after undergoing some fluctuations for l values between 40 and 70. The spectrum for direct electrons (black dots) is included as a reference. As it can be seen, both the standard Keldysh amplitude and the fully quantum mechanical result that incorporates rescattering exhibit very similar electron yields for energies lower than $2.5U_p$ where the spectrum is consisting only of direct electrons. As the electron energy increases, the rescattered electrons begin to exceed the direct ones and the curves start to differ from each other. The transition probability, consisting almost exclusively of rescattered electrons, reaches a plateau consisting of

a sequence of suppressions separated by rounded tops. This behaviour is a direct consequence of quantum interference, as the released electrons interfere constructively and destructively in every optical cycle of the laser field as a function of energy. For large energies of about $10U_p$ the plateau shows a cutoff that indicates the end of the rescattering spectrum. The position of this cutoff as well as the onset energy of the plateau fluctuate with the orientation of the emitted electrons with respect to the electric field of the laser as well as with variations of the intensity of the field [11, 21, 22].

4.3.2 Ionization spectrum for the $1b_1$ and $1b_2$ orbitals of H_2O

The study on the H_2O molecular orbitals presented in Chapter 3 is extended in this section with the aim of exploring the ATI spectrum of the $1b_1$ and $1b_2$ molecular orbitals previously characterized as spherical orbitals. The zero-range model calculation carried out in the previous section combined with the strong field approximation is applied to these valence orbitals in order to explore their response to an intense laser field.

Each molecular orbital is treated as an independent atom in which the eigenvalues ϵ_{1b_1} and ϵ_{1b_2} obtained from the radial representation of their effective potentials, $V_{\text{eff}}(r)$, are considered their binding energies, respectively. With this in mind, it is possible to generate the ionization spectrum for direct electrons and that for rescattering electrons that would correspond to each molecular orbital under a strong laser field. Inserting the molecular binding energies into Eqs. (4.5) and (4.8) one can explore the convergence of the ionization spectrum in terms of the number of Bessel functions included in their respective sums.

Similarly to the case of strong field ionization of a He atom, the quadrature $F(l)$ in (4.11) remains to be solved in order to obtain the ionization spectrum for rescattered electrons. The general expression (4.8), which encloses the limiting case of ionization of direct electrons, generates an electron yield which follows that of direct electrons for low energies, i.e., electrons energies for which the direct spectrum is not vanished and the rescattering effects are not taken into account. This section is aimed to validate the previous statement and explore the convergence of the ATI spectrum of these two simplified representations of H_2O orbitals.

Figures 4.5 and 4.6 show the values taken by the function $F(l)$ for a set of values of $l_{\max}$, $l_{\max} = 30, \ldots, 80$, that indicate the extension of the sum (4.8) in terms of Bessel functions and the

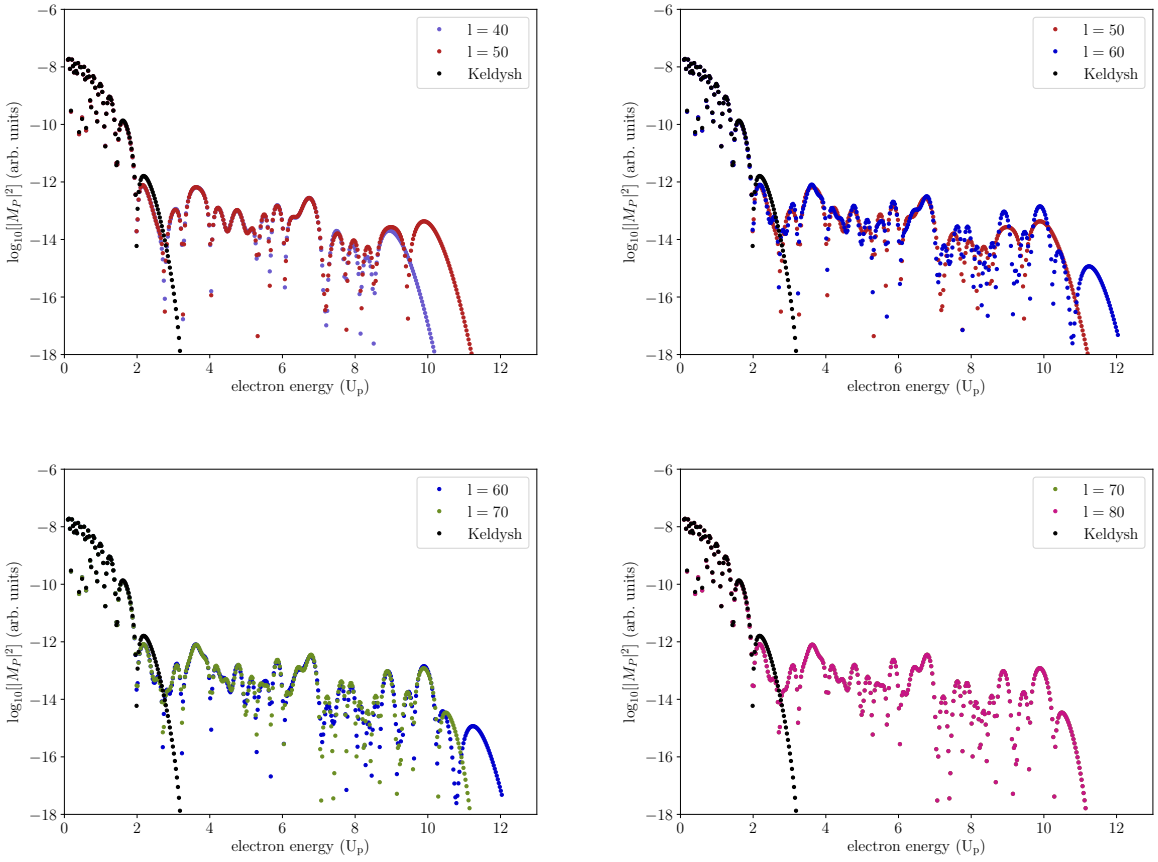

Figure 4.4: ATI spectrum of a zero-range He model with a binding energy of $E_0 = -0.9$ a.u. by a linearly polarized field with a laser intensity of 10^{15} W/cm^2 with $\hbar\omega = 1.58$ eV in terms of an increasing Bessel order, $l_{\max}$, as a function of the electron energy (in colour). The result from the standard Keldysh approximation is shown as the black dotted line.

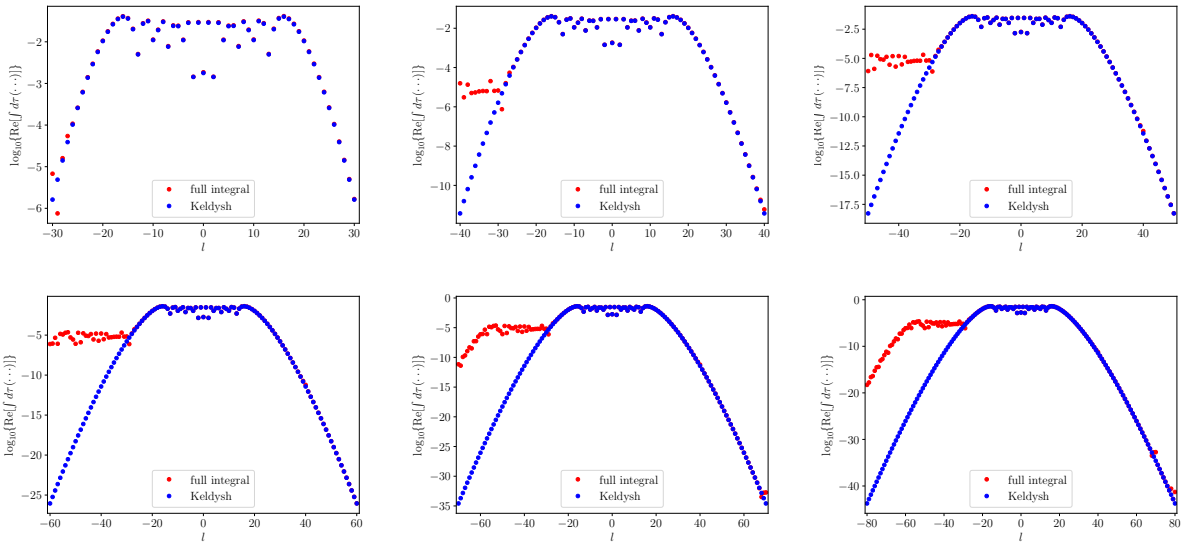

Figure 4.5: Numerical evaluation of the time integral $F(l)$ in the transition amplitude (4.11) (red dots) in contrast with its analogous Bessel term in the Keldysh amplitude for direct transmission (blue dots) for the $1b_1$ MO of H_2O as a function of the Bessel function order l for increasing values of $l_{\max}$, $l = [-l_{\max}, \ldots, l_{\max}]$.

Bessel term in the standard Keldysh amplitude (4.5) in red and blue, respectively. The numerical values of the integral $F(l)$ were rescaled for both molecular orbitals, divided by a factor of 5.5 for the $1b_1$ MO and by a factor of 6.5 for the $1b_2$ MO, in order to make the comparability between the curves visible. Correspondingly, the working precision of the calculations was gradually increased for $|l| > 0$ up to a maximum of 50 digits of precision for $l_{\max} = 80$. As it has been observed for ionization along the electric field of the laser for a He atom [11], the precise agreement between the emission rate for direct electrons and the full ionization spectrum including rescattering for energies below the cutoff of the direct-electron spectrum indicates that a correlation between the red and blue curves should be expected for a range of values of $l_{\max}$ before deviations due to rescattering become substantial. This behaviour can be observed for both molecular orbitals for $l < -30$, where the quadrature $F(l)$ reaches a plateau at about 10^{-5} that extends up to about $l < -60$ where signs of convergence of the time integral $F(l)$ become noticeable as the red curve begins to decline.

The ionization spectra corresponding to the $1b_1$ and $1b_2$ molecular orbitals are shown in

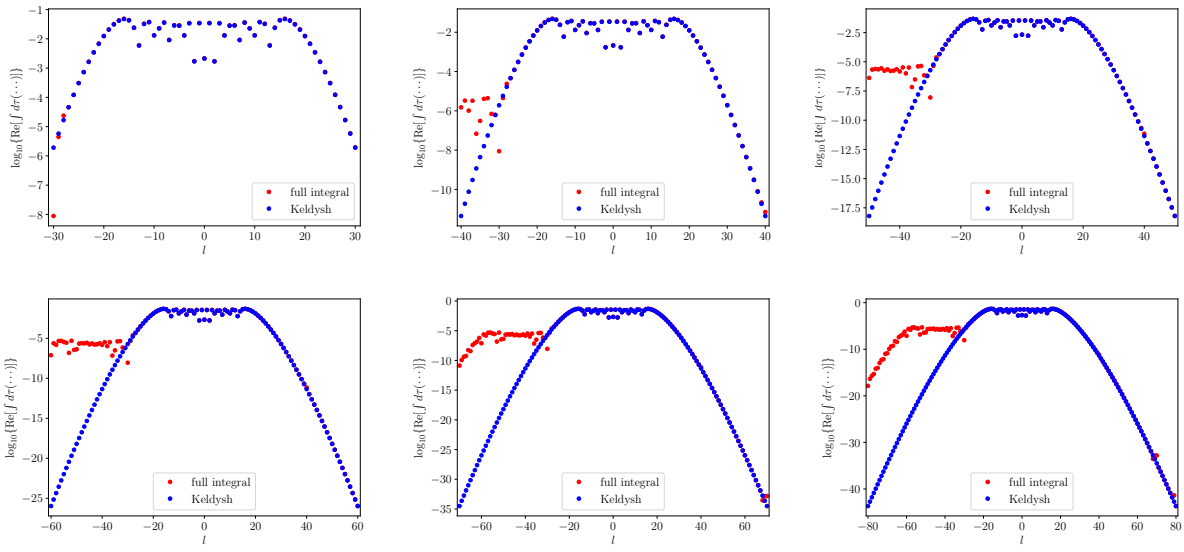

Figure 4.6: Numerical evaluation of the time integral $F(l)$ in the transition amplitude (4.11) (red dots) in contrast with its analogous Bessel term in the Keldysh amplitude for direct transmission (blue dots) for the $1b_2$ MO of H_2O as a function of the Bessel function order l for increasing values of $l_{\max}$, $l = [-l_{\max}, \ldots, l_{\max}]$.

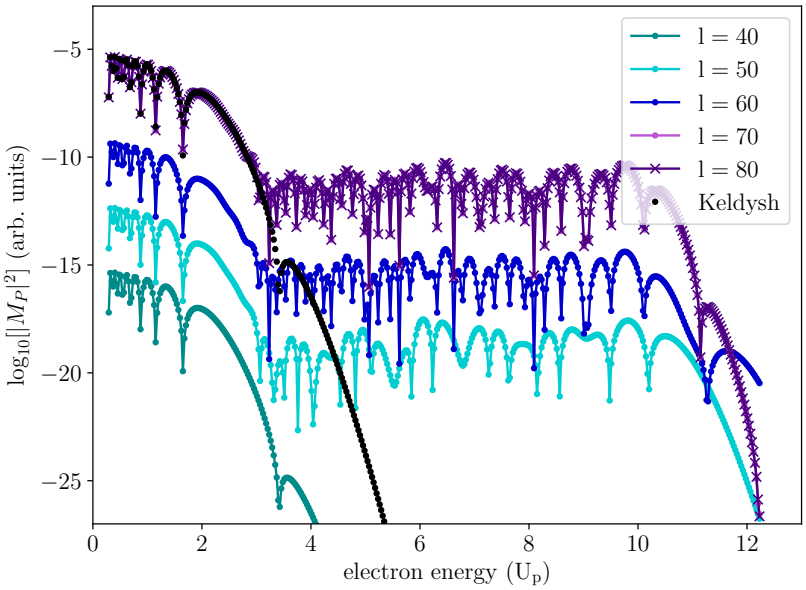

Figure 4.7: ATI spectrum for the $1b_1$ MO of H_2O by a linearly polarized field with laser intensity of 10^{15} W/cm^2 with $\hbar\omega = 1.58$ eV in terms of an increasing Bessel order, l, as a function of the electron energy (in colour). The result from the standard Keldysh approximation is shown as the black dotted line.

Figures 4.7 and 4.8 as a function of the electron energy. The evolution of the electron yield is presented in terms of the Bessel order l, $40 \leq l \leq 80$. As it can be noticed, expanding the sum in Eq. (4.8) up to $l_{\max} = 80$, purple curve, leads to convergence of the ATI spectrum for both molecular orbitals. Consistently with the comparison with the standard Keldysh amplitude shown in Figures 4.5 and 4.6, as l increases a higher working precision is needed to obtain an accurate representation of the transmission amplitude. It can be seen that the final shape of the spectrum for low energies can be obtained for l values as low as 40. For those energy values one obtains full agreement between the transmission due to direct electrons only (black curve) and the spectrum of rescattered electrons. As the electron energy increases, the Keldysh amplitudes corresponding to both orbitals $1b_1$ and $1b_2$ vanish, giving rise to the onset of the plateau that describes the spectrum consisting entirely of rescattered electrons.

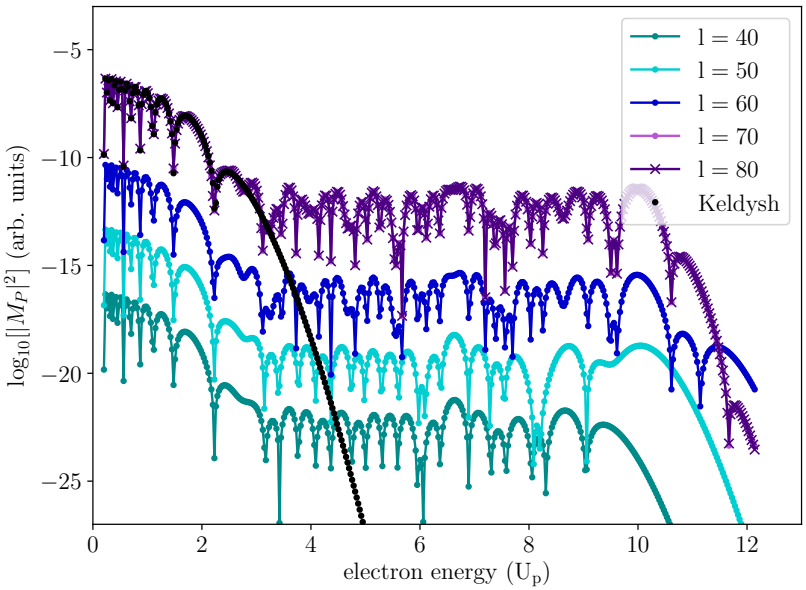

Figure 4.8: ATI spectrum for the $1b_2$ MO of H_2O by a linearly polarized field with laser intensity of 10^{15} W/cm^2 with $\hbar\omega = 1.58$ eV in terms of an increasing Bessel order, l, as a function of the electron energy (in colour). The result from the standard Keldysh approximation is shown as the black dotted line.

5 Saddle point approximation

For laser fields of sufficiently high intensity, the ATI spectrum can be generated by implementing a saddle point evaluation [ref spa] of the multidimensional integral for the transition amplitude obtained in the previous chapter. This semi-classical approximation provides a deeper physical insight than the expansion in Bessel functions from the improved Keldysh approximation, and establishes a connection between the process of ATI of an electron with the concept of quantum paths, which represent space-time trajectories of the tunneling electrons. This concept has its origins in the alternative formulation of quantum mechanics introduced by Feynman in terms of path integrals [23], where the probability amplitude of a quantum mechanical process can be represented as a coherent superposition of contributions from all possible spatio-temporal paths that connect the initial and final state of the system.

The analysis presented in this chapter establishes the connection between the quantum mechanical path integral formalism and the improved Keldysh approximation discussed in Sec. 4.2. The transition amplitude that describes the ionization of an electron under an external laser field is evaluated within the two frameworks, that in which only direct electrons are considered as well as the case that incorporates rescattering to the parent ion.

5.1 Quantum path analysis

In the length gauge the compact form of the Volkov state can be expressed as

$$|\psi_{\mathbf{p}}^{(V)}(t)\rangle = \quad |\mathbf{p} - e\mathbf{A}(t)\rangle e^{-iS_{\mathbf{p}}(t)}, \tag{5.1}$$

where $|\mathbf{p} - e\mathbf{A}(t)\rangle$ represents a plane-wave state and $S_{\mathbf{p}}(t) = 1/2m \int^{t} d\tau [\mathbf{p} - e\mathbf{A}(\tau)]^2$ denotes the action of the system. Consequently, the Volkov time-evolution operator can be written down in

the form of an expansion in terms of its Volkov states

$$U^{(V)}(t,t') = \int d^3\mathbf{k} |\psi^{(V)}_{\mathbf{k}}(t)\rangle\langle\psi^{(V)}_{\mathbf{k}}(t')|. \tag{5.2}$$

Inserting the expansion (5.2) into the matrix element (4.7) and given the time dependence of the ground state wave function, $|\psi_0(t)\rangle = \exp(iE_0 t)|\psi_0\rangle$, we may write

this is from the literature!

$$\begin{aligned} M_{\mathbf{p}} = & \int_{-\infty}^{\infty} dt \int_{-\infty}^{t} \int d^3\mathbf{k}\ \langle \mathbf{p} - e\mathbf{A}(t)|V|\mathbf{k} - e\mathbf{A}(t)\rangle\ \langle \mathbf{k} - e\mathbf{A}(t')|V|\psi_0\rangle \\ & \times \exp\left[i \left(-\frac{1}{2m}\int_{t}^{\infty} d\tau [\mathbf{p} - e\mathbf{A}(\tau)]^2 - \frac{1}{2m}\int_{t'}^{t} d\tau [\mathbf{k} - e\mathbf{A}(\tau)]^2 + \int_{-\infty}^{t'} d\tau |E_0| \right) \right] \\ \sim & \int_{\infty}^{\infty} dt \int_{-\infty}^{t} dt' \int d^3\mathbf{k} \exp\left[iS_{\mathbf{p}}(t,t',\mathbf{k}) \right] m_{\mathbf{p}}(t,t',\mathbf{k}). \end{aligned} \tag{5.3}$$

As one may notice, the action in the exponent, $S_{\mathbf{p}}(t,t',\mathbf{k})$, consists of three parts which correspond to the action of the entire system after rescattering, between ionization and rescattering and before ionization.

It is revealing to point out the contrast of the ionization amplitude (5.3) obtained with the strong field approximation with its analogous representation in terms of Feynman's theory of path integral. The time evolution operator of the entire system has the path integral representation

$$U(\mathbf{r}t, \mathbf{r}'t') = \int_{(\mathbf{r}',t')\to(\mathbf{r},t)} \mathcal{D}[\mathbf{r}(\tau)]\, e^{iS(t,t')}, \tag{5.4}$$

where $S(t,t') = \int_{t'}^{t} d\tau \mathcal{L}[\mathbf{r}(\tau),\tau]$ is the action calculated along a specific path by integrating the Lagrangian of the entire system along that path, and the integral measure denoted by $\mathcal{D}[\mathbf{r}(\tau)]$ establishes a coherent sum over all possible paths that connect $(\mathbf{r}t)$ and $(\mathbf{r}'t')$, independently of whether or not the paths might be followed by the actual system. In contrast, by implementing the strong field approximation we have approximated the exact action of the system at the various stages of the process: before ionization, in between ionization and rescattering, and after rescattering, as (5.3) indicates, where the ionization amplitude is computed through a sum over the exponential of the action over a five-parameter set of paths, parametrized by the ionization time t', the rescattering time t and the canonical momentum of the orbit in between $\mathbf{k}$ [24].

The five-dimensional set of paths over which the transition amplitude (5.3) is evaluated can be reduced further by implementing a saddle point approximation of the integral, in which a

handful of relevant paths remains to be considered. In this process, the transition amplitude (5.3) is approximated by expanding the phase about its stationary points, saddle points. The condition

$$\frac{\partial S}{\partial q_i} = 0 \tag{5.5}$$

where $q_i (i = 1, \ldots, 5)$ runs over the five variables t, t' and $\mathbf{k}$, leads to the saddle-point equations [24, 25]

$$\begin{aligned} \left(\mathbf{k} - e\mathbf{A}(t')\right)^2 &= -2m|E_0| \\ \left(\mathbf{k} - e\mathbf{A}(t)\right)^2 &= \left(\mathbf{p} - e\mathbf{A}(t)\right)^2 \\ (t - t')\mathbf{k} &= \int_{t'}^{t} d\tau e\mathbf{A}(\tau). \end{aligned} \tag{5.6}$$

The solutions $(t_S(\text{Re } t_S > \text{Re } t'_S), t'_S, \mathbf{k}_S)$, are known as the stationary points of the quasicassical action of the system, and define the quantum orbits over which the time integral in (5.3) needs to be carried out. From a physical perspective, Eqs. (5.6) ensure the energy conservation at the time of tunneling, elastic scattering of the electron into its final state when it returns, and that in fact the electron returns to its parent ion, respectively. Since $|E_0| > 0$ in (5.6), the condition of energy conservation at the time of ionization cannot be satisfied for any real time t'. As a consequence, the solutions $(t_S, t'_S, \mathbf{k}_S)$ of the saddle-point equations describe complex orbits which restrains a straightforward visualization of the trajectories.

The matrix element (5.3) can now be expressed in terms of the saddle point solutions as

$$M_{\mathbf{p}} \sim \sum_i \left(\frac{(2\pi i\hbar)^5}{\det(\partial^2 S/\partial q_j \partial q_k)_{j,k=1,\ldots,5}} \right)^{1/2} \times \exp(iS(t_{S_i}, t'_{S_i}, \mathbf{k}_{S_i})), \tag{5.7}$$

where $q_i (i = 1, \ldots, 5)$ runs over the five variables t_S, t'_S and $\mathbf{k}_S$. The sum (5.7) considers a subset of trajectories which determine the shape of the ionization spectrum through their interferences, constructive or destrutive.

5.2 Results

5.2.1 Direct trajectories

5.2.2 Trajectories with rescattering

6 Conclusions

Bibliography

[1] Susana Arias Laso and Marko Horbatsch. Calculation of stark resonance parameters for valence orbitals of the water molecule. *Phys. Rev. A*, 94:053413, 2016. 1

[2] P. Agostini, F. Fabre, G. Mainfray, G. Petite, and N. K. Rahman. Free-free transitions following six-photon ionization of xenon atoms. *Phys. Rev. Lett.*, 42:1127–1130, 1979. 4

[3] L. V. Keldysh. Ionization in the field of a strong electromagnetic wave. *Soviet Physics JETP*, 20:1307–1314, 1965. 4, 5, 7

[4] M. J. Nandor, M. A. Walker, L. D. Van Woerkom, and H. G. Muller. Detailed comparison of above-threshold-ionization spectra from accurate numerical integrations and high-resolution measurements. *Phys. Rev. A*, 60:R1771–R1774, 1999. 4

[5] Armin Scrinzi, Michael Geissler, and Thomas Brabec. Ionization above the coulomb barrier. *Phys. Rev. Lett.*, 83:706–709, 1999. 4

[6] C.J. Joachain, M. Dörr, and N. Kylstra. *High-Intensity Laser-Atom Physics*, volume 42 of *Advances In Atomic, Molecular, and Optical Physics*. Academic Press, 2000. 4

[7] W. Becker, F. Grasbon, R. Kopold, D.B. Milošević, G.G. Paulus, and H. Walther. *Above-Threshold Ionization: From Classical Features to Quantum Effects*, volume 48 of *Advances In Atomic, Molecular, and Optical Physics*. Academic Press, 2002. 4, 6

[8] F. H. M. Faisal. Collision of electrons with laser photons in a background potential. *Journal of Physics B: Atomic and Molecular Physics*, 6(11):L312–L315, 1973. 4

[9] Howard R. Reiss. Effect of an intense electromagnetic field on a weakly bound system. *Phys. Rev. A*, 22:1786–1813, 1980. 4

[10] J Z Kaminski and F Ehlotzky. Relation between sidelobes and coulomb corrections in high-order above-threshold ionization. *Journal of Physics B: Atomic, Molecular and Optical Physics*, 30(1):69–76, 1997. 4

[11] A. Lohr, M. Kleber, R. Kopold, and W. Becker. Above-threshold ionization in the tunneling regime. *Phys. Rev. A*, 55:R4003–R4006, 1997. 4, 5, 6, 7, 13, 15

[12] B. Walker, B. Sheehy, L. F. DiMauro, P. Agostini, K. J. Schafer, and K. C. Kulander. Precision measurement of strong field double ionization of helium. *Phys. Rev. Lett.*, 73: 1227–1230, Aug 1994. 5

[13] B. Walker, B. Sheehy, K. C. Kulander, and L. F. DiMauro. Elastic Rescattering in the Strong Field Tunneling Limit. *Phys. Rev. Lett.*, 77:5031–5034, 1996. 5

[14] Zi Jian Long and Wing-Ki Liu. Keldysh theory of strong field ionization. *Can. J. Phys.*, 88: 227–245, 2010. 6

[15] W. Becker, A. Lohr, M. Kleber, and M. Lewenstein. A unified theory of high-harmonic generation: Application to polarization properties of the harmonics. *Phys. Rev. A*, 56: 645–656, 1997. 6

[16] W Becker, A Lohr, and M Kleber. Effects of rescattering on above-threshold ionization. *Journal of Physics B: Atomic, Molecular and Optical Physics*, 27(14):L325–L332, jul 1994. 6

[17] Yu. N. Demkov and V. N. Ostrovskii. *Zero-Range Potentials and Their Applications in Atomic Physics*. Physics of Atoms and Molecules. Springer US, New York, 1988. ISBN 978-1-4684-5453-6. 6

[18] S. V. Borzunov, M. V. Frolov, M. Yu. Ivanov, N. L. Manakov, S. S. Marmo, and Anthony F. Starace. Zero-range-potential model for strong-field molecular processes: Dynamic polarizability and photodetachment cross section. *Phys. Rev. A*, 88:033410, 2013. 6

[19] M. Kleber. Exact solutions for time-dependent phenomena in quantum mechanics. *Physics Reports*, 236(6):331 – 393, 1994. ISSN 0370-1573. 7

[20] W. Becker, S. Long, and J. K. McIver. Short-range potential model for multiphoton detachment of the H^- ion. *Phys. Rev. A*, 42:4416–4419, Oct 1990. 7

[21] G. G. Paulus, W. Nicklich, Huale Xu, P. Lambropoulos, and H. Walther. Plateau in above threshold ionization spectra. *Phys. Rev. Lett.*, 72:2851–2854, 1994. 13

[22] G. G. Paulus, W. Becker, W. Nicklich, and H. Walther. Rescattering effects in above-threshold ionization: a classical model. *Journal of Physics B: Atomic, Molecular and Optical Physics*, 27(21):L703–L708, 1994. 13

[23] R. P. Feynman. Space-time approach to non-relativistic quantum mechanics. *Rev. Mod. Phys.*, 20:367 – 387, 1948. 19

[24] R. Kopold, W. Becker, and M. Kleber. Quantum path analysis of high-order above-threshold ionization. *Optics Communications*, 179(1):39 – 50, 2000. 20, 21

[25] M. Lewenstein, K. C. Kulander, K. J. Schafer, and P. H. Bucksbaum. Rings in above-threshold ionization: A quasiclassical analysis. *Phys. Rev. A*, 51:1495–1507, 1995. 21